Journal of Data Science 0 (0), 1–18
??? 2024
DOI: 10.6339/24-JDS1145
Data Science in Action

Mixed Model and Gaussian Process to Investigate the External Influence on the Propagation Time of Ultrasonic Waves on Masonry Walls

Rosineide Fernando da Paz[1,*], Daiane Aparecida Zuanetti[2],
Renan Vinicius Rodrigues[2], and Esequiel Mesquita[1]

[1]*Universidade Federal do Ceará, Campus of Russas, Ceará, Brazil*
[2]*Universidade Federal de São Carlos, Statistical Departament, São Carlos, São Paulo, Brazil*

Abstract

The ultrasonic testing has been considered a promising method for diagnosing and characterizing masonry walls. As ultrasonic waves tend to travel faster in denser materials, their use is common in evaluating the conditions of various materials. Presence of internal voids, e.g., would alter the wave path, and this distinct behavior could be employed to identify unknown conditions within the material, allowing for the assessment of its condition. Therefore, we applied mixed models and Gaussian processes to analyze the behavior of ultrasonic waves on masonry walls and identify relevant factors impacting their propagation. We observed that the average propagation time behavior differs depending on the material for both models. Additionally, the condition of the wall influences the propagation time. Gaussian process and mixed model performances are compared, and we conclude that these models can be useful in a classification model to automatically identify anomalies within masonry walls.

Keywords *automated monitoring; characterization of masonry; non-destructive test; statistical application*

1 Introduction

Non-Destructive Testing (NDT) is a tool for analyzing the stability and quality of masonry constructions, detecting internal structural problems without causing any damage to their structure. Due to this characteristic, this method can prevent unnecessary expenses and destruction of the analyzed structure. NDT has gained notoriety in recent years due to its non-destructive nature. Additionally, the use of ultrasonic waves has been one of the methods employed to perform NDT (Kot et al., 2021).

The non-invasive nature and high sensitivity of the acoustic emission technique have attracted the attention of researchers for monitoring structures made of various materials to detect damages. Particularly in civil engineering, this tool has shown promise in recent years and can be utilized for diagnosing structural damage in masonry structures, as described in Verstrynge et al. (2021) and its references.

Among others, ultrasonic testing (UT) has been considered a promising method for diagnosing and characterizing masonry walls. Some studies and applications can be found, for example,

*Corresponding author. Email: rfdapaz@ufc.br.

Received February 12, 2024; Accepted July 2, 2024

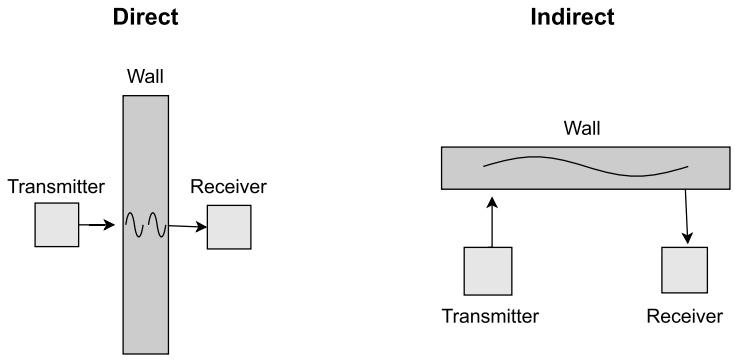

Figure 1: Direct ultrasonic test, on the left side of the figure, involves wave emission and reception points on opposite faces of the wall. On the right side of the figure, the indirect ultrasonic test presents wave emission and reception points on the same side of the wall.

in Araújo et al. (2020); Valluzzi et al. (2018); Binda et al. (2003). This method involves the use of elastic waves, which can be obtained either by ultrasonic impulses generated by the damage itself (in monitoring) or by using a transmitter at a specific point in the structure. The present work focuses on the ultrasonic test involving elastic waves emitted by transmitters. In this case, each emitted wave is collected by the receiver. Subsequently, the propagation time that the wave took from the emission point to the reception point is measured. As ultrasonic waves tend to travel faster in denser materials, voids, for example, would alter the wave path. This characteristic can be utilized to identify unknown conditions within the material and enable the evaluation of its condition.

Despite being a promising method, there are numerous challenges in using UT for the evaluation and monitoring of masonry walls due to material heterogeneity and interference from external factors like noise, humidity, and measurement height. Some of these factors can be standardized during tests, such as humidity and noise. However, other factors must be taken into account in the analysis, including measurement height and material heterogeneity.

Another challenge concerns the fact that it is not always possible to conduct a direct ultrasonic test for existing buildings. In the direct test, the emitter and receiver are positioned on opposite sides of the wall, as shown on the left side of Figure 1. Conversely, the indirect test is conducted with the wave transmitter and receiver placed on the same side of the analyzed element, as shown on the right side of Figure 1. Additional types of ultrasonic testing for masonry elements can be explored in Miranda et al. (2013).

In the context of indirect ultrasonic testing, Zuanetti et al. (2021) shows exploratory results that provides evidence that ultrasonic waves may not penetrate the wall under the presence of internal voids, resulting in faster propagation than expected in such conditions, due to the wave propagating faster in the surface mortar. This situation can lead traditional analyses, which are based on correlations through heat maps, to draw wrong conclusions, since the wave, when entering the wall, propagates more slowly in the air than in solid parts of the material. Therefore, in this situation, more sophisticated statistical models must be employed to analyze the atypical wave trajectory behavior, without relying only on the physical parameters of the materials, and to identify factors that impact wave behavior, such as the height at which measurements are taken and the different types of materials that make up the wall, among others. This procedure plays a crucial role in developing expert systems designed for automated monitoring operations.

Building on theses issues, the goal of this work is to study and understand how ultrasonic waves behave inside massive masonry, observing and describing the general variations in their propagation time on walls under different conditions and, thus, understand how the wall conditions reflect on the behavior of the wave. Here, we analyze wave propagation time curves through masonry walls using mixed models (Rodrigues, 2009; Edwards et al., 2006; Singer and Andrade, 1986; Laird and Ware, 1982) and Gaussian processes (Cheng et al., 2019; Quintana et al., 2016; Ebden, 2015; Banerjee et al., 2008; Williams and Rasmussen, 2006), which are traditional methodologies in the analysis of longitudinal data or repeated measures, and compare their inferential and predictive results. These methodologies model the existing association between measurements taken from the same wave and allow a nonlinear relationship between the propagation time and the traveled distance.

Beside the structural equation modeling framework, the mixed model is also an important tool for fitting growth curves (Grimm et al., 2016) where the relative standing of an individual at each time is modeled as a function of a growth process, and allows the best parameter values for that growth process being fitted to each individual. The growth process may be linear or nonlinear with respect to time, time-invariant covariates or to random effects. The methodology can be used to investigate systematic change, or growth, and inter-individual variability in this change. In the 2000s there were also innovations in how growth models could be used to simultaneously model individual changes and examine time-dependent lead-lag associations with longitudinal data (Grimm et al., 2007, 2013).

Thus, the present work primarily applies mixed models and Gaussian process to analyze the influence of height measurements and internal voids on the propagation time of a wave in masonry and compare the results, their advantages and disadvantages. The dataset used here was initially statistically analyzed by Zuanetti et al. (2021) with the aim of clustering. However, a study on external influences has not been carried out.

Based on the results found, we conclude that both models identify the nonlinearity of the relationship between the distance traveled by an ultrasonic wave and its propagation time in masonry walls. Additionally, the Gaussian process indicates that the wave propagates faster in bricks with voids inside, providing evidence that the wave can propagate through the wall coating if there is a void in its way. Furthermore, it is possible that this model produces good results in a classification model. This procedure plays a crucial role in developing expert systems designed for automated monitoring operations.

The remainder of the manuscript is organized as follows. Section 2 describes the experiment and the data set to be analyzed. Section 3 introduces the statistical models used in the analysis and how to carry out out-of-sample prediction with them. Section 4 shows the results. Finally, Section 5 shows a final discussion about the observed results.

2 Ultrasonic Waves for Non-destructive Test in Masonry Wall

In this section, we present the experimental data obtained from walls built to mimic old constructions usually found in the Ceará State of Brazil. The experiment was conducted using two identical walls built in a laboratory, both with dimensions of 1.50 meters (height) × 1.00 meter (width) × 0.135 meters (thickness). The materials used for building them were ceramic bricks and grout, which are commonly used in masonry constructions in Brazil. One wall was built in a regular way, without damages, and the other has voids to simulate a damage building. Figure 2 (Rodrigues, 2021b) shows the original walls (experimental panels) before

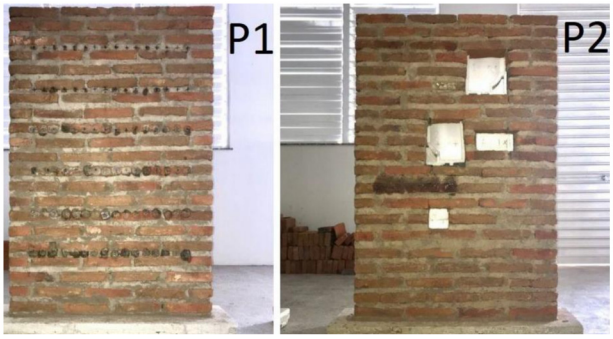

Figure 2: Wall specimens (original panels) used in the experiment (Rodrigues, 2021b).

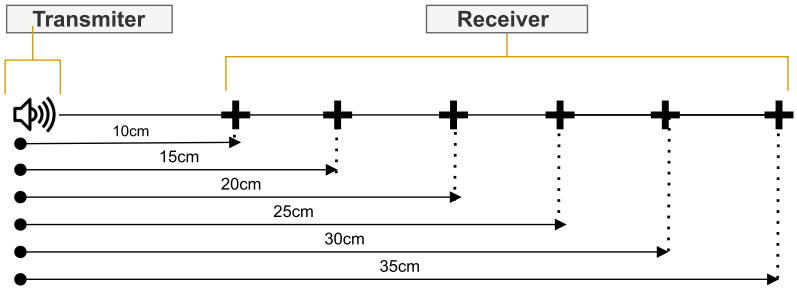

Figure 3: Wave transmission and reception diagram.

being coated with grout. Panel P1 is the full wall without damages, while panel P2 contains voids.

The full and damaged walls were coated using the grout commonly used in masonry buildings in Brazil. Then, following the norm of civil engineering (ABNT, 2020), see Mesquita et al. (2018), the walls were divided into 12 frames (Q1, Q2, . . . , Q12) drawn to contain the locations for the six propagation time measurements of the wave (the points where the sound signals were emitted and received were demarcated in each frame of the both panels). The frames were drawn with a border of 10 cm at the top, right, and left of the demarcations, and 20 cm below the demarcations.

A wave was emitted from the left corner of each frame, over the first demarcation. The propagation time was measured on a horizontal line 10 cm from the emission for the first measurement, and an additional 5 cm for each subsequent measurement. Figure 3 shows the diagram for the experiment where '+' represents the location where the waves were received. In this figure, it is possible to see each distance traveled by the wave for each propagation time measurement: 10 cm, 15 cm, and so on.

For each frame and wall, 10 ultrasonic waves (replications) were emitted and received, totaling 240 waves. Each wave contains six points of measurement, one for each distance (10, 15, 20, 25, 30, 35 cm). That is, the ith wave provides a vector of data $(y_{i1}, y_{i2}, y_{i3}, y_{i4}, y_{i5}, y_{i6})^T$, where each component records the propagation time to that distance. Here, each vector that contains a sequence of six propagation time measurements of a wave is called an "individual". The measurements of a specific wave (individual) are highly correlated with each other, and if the traveled material is homogeneous, the relationship between the time and the distance traveled

by the wave should be linear. However, the material used in a masonry wall is not homogeneous.

In the study, we have $m = 230$ observed curves (representation of individuals), since nine waves were not captured by the receiver in any distance and one of them with only 4 measurements instead of 6 was omitted. As previously mentioned, the material that makes up the walls is not homogeneous and the relationship between distance traveled and propagation time appears to be nonlinear for many waves, as will be shown in results section. Thus, to analyze the produced data, we must use a statistical model that considers the correlation between the observations and the nonlinearity of the data. In exploratory results, comparing the smoothed average curves for waves from the wall without voids and for the wall with voids separated by void in wave trajectory and without void in wave trajectory, but in its frame, Zuanetti et al. (2021) observe that up to around 22.5 cm (approximately where first voids are found) the average curves are very similar and, sometimes, waves propagated on the brick with voids are a little slower. After the distance of 22.5 cm, the average curves are more distant and the curve representing waves in voids takes less time to be captured, i.e., they are faster in average.

Based on the above, the present work proposes the use of statistical methods that consider and model these specific characteristics of the data set. With the fitted models, it is possible to analyze the influence of height measurements, presence of internal voids and many other building features on the propagation time curve. Additionally, a study is carried out on the behavior of the wave in different wall materials and we compare mixed model and Gaussian process results what is not common in literature.

3 Models for Analyzing Correlated Nonlinear Data

Traditional and useful models for analyzing correlated data from repeated measures or longitudinal data include mixed models (MM) and Gaussian processes (GP). In this section, these models are briefly defined for nonlinear data. Additionally, it is explained how they are used to identify the relevant features and factors that impact the investigated response. The models are estimated under the Bayesian perspective, since the Gaussian process is often estimated under this view and we want to compare its results with the results of the mixed model. In addition, in general, Bayesian estimation does not present convergence problems even for models with a greater number of random effects.

3.1 Mixed Models

A widely used model to consider intra-individual correlation in the dataset and to describe the behavior of a response variable over its measurements is the mixed model with fixed and random effects. Let $\boldsymbol{y} = (\boldsymbol{y}_1^T, \ldots, \boldsymbol{y}_m^T)^T$ be the observed data for m individuals where $\boldsymbol{y}_i = (y_{i1}, \ldots, y_{in_i})^T$, for $i = 1, \ldots, m$, with y_{ij} being the observation of the ith individual in the jth measurement of the experiment, for $j = 1, \ldots, n_i$. In this study, y_{ij} is the observed propagation time of the ith ultrasonic wave at the jth distance, for $i = 1, \ldots, 230$ and $j = 1, \ldots, 6$.

A linear mixed model for each individual is traditionally defined as

$$\boldsymbol{Y}_i = \boldsymbol{X}_i\boldsymbol{\beta} + \boldsymbol{Z}_i\boldsymbol{b}_i + \boldsymbol{\epsilon}_i, \text{ for } i = 1, 2, \ldots, m,$$

where $\boldsymbol{\beta}$ is the $(p \times 1)$ vector of fixed effects; $\boldsymbol{X}_i$ is the $(n_i \times p)$ design matrix associated with fixed effects; $\boldsymbol{b}_i$ is the $(q \times 1)$ vector of random effects for the ith individual; $\boldsymbol{Z}_i$ is the $(n_i \times q)$ design matrix associated with random effects for the ith individual and $\boldsymbol{\epsilon}_i$ is the $(n_i \times 1)$ vector of random

errors for the ith individual. Usually, we assume that $\boldsymbol{b}_i \sim Normal(\mathbf{0}, \boldsymbol{G})$ and $\boldsymbol{\epsilon}_i \sim Normal(\mathbf{0}, \boldsymbol{R}_i)$, where $\boldsymbol{G}$ is the $(q \times q)$ variance–covariance matrix for the random effects; $\boldsymbol{R}_i$ is the $(n_i \times n_i)$ variance–covariance matrix for the random errors and $\mathbf{0}$ is a $(q \times 1)$ null vector for $\boldsymbol{b}_i$ and $(n_i \times 1)$ null vector for $\boldsymbol{\epsilon}_i$. The variables associated with fixed and random effects in the studied case are specified in the next section.

If we assume that $\boldsymbol{b}_i$ and $\boldsymbol{\epsilon}_i$ are independent, $E(\boldsymbol{Y}_i) = \boldsymbol{X}_i\boldsymbol{\beta}$ and $Var(\boldsymbol{Y}_i) = \boldsymbol{Z}_i\boldsymbol{G}\boldsymbol{Z}_i^T + \boldsymbol{R}_i$ or $E(\boldsymbol{Y}_i|\boldsymbol{b}_i) = \boldsymbol{X}_i\boldsymbol{\beta} + \boldsymbol{Z}_i\boldsymbol{b}_i$ and $Var(\boldsymbol{Y}_i|\boldsymbol{b}_i) = \boldsymbol{R}_i$. In this work, we set $\boldsymbol{R}_i = \sigma^2\mathbf{I}$, where $\mathbf{I}$ represents an identity matrix, and an unstructured matrix for $\boldsymbol{G}$, which are traditional choices for a mixed model. Note that as the marginal variance of $\boldsymbol{Y}_i$ depends on the variables associated with the random effects and their covariance matrix, the mixed model may be a heteroscedastic model. We discuss this further in the results.

Adopting a Bayesian approach for estimating this model, we assume that

- $\phi = \frac{1}{\sigma^2} \sim Gamma(\lambda_1, \lambda_2)$;
- $\boldsymbol{G} \sim Inverse - Wishart_q(v, \boldsymbol{W})$; and
- $\boldsymbol{\beta} \sim Normal_p(\mathbf{0}, \sigma_\beta^2\mathbf{I})$,

where $\lambda_1 > 0$, $\lambda_2 > 0$, $v > q - 1$, positive definite $\boldsymbol{W}$ and $\sigma_\beta^2 > 0$ are known hyperparameters and the $Gamma$ distribution is parameterized such that $E[\phi] = \frac{\lambda_1}{\lambda_2}$.

These prior distributions and the prior distribution for the random effects are conjugate to the $Normal$ model assumed for the random error, and the full conditional posterior distributions are available in closed form (Rodrigues, 2021a). Therefore, a Gibbs sampling algorithm may be applied to simulate samples from the joint posterior distribution. In this model, a nonlinear relationship between the traveled distance and the propagation time may be included through a polynomial function between these variables.

3.2 Gaussian Process

An alternative statistical model that also considers related observations and allows a nonlinear relationship between them is the Gaussian process. A collection of random variables $\{\eta(d_1), \eta(d_2), \ldots\}$, indexed by elements $d_1, d_2, \ldots$, defines a Gaussian process (GP) if any finite subset of them follows a $Normal$ multivariate distribution. In other words, $\eta(\cdot) \sim \text{GP}(m(\cdot); K(\cdot,\cdot))$ if

$$\big(\eta(d_{j_1}), \eta(d_{j_2}), \ldots, \eta(d_{j_n})\big)^T \sim Normal_n\big(m(\boldsymbol{D}); K(\boldsymbol{D}, \boldsymbol{D})\big), \tag{1}$$

for any finite subset $\boldsymbol{D} = (d_{j_1}, d_{j_2}, \ldots, d_{j_n})^T$. Here, due to the context of repeated measures, we have

$$\big(\eta(d_{i1}), \eta(d_{i2}), \ldots, \eta(d_{in_i})\big)^T \sim Normal_{n_i}\big(m(\boldsymbol{D}_i); K_i(\boldsymbol{D}_i, \boldsymbol{D}_i)\big), \tag{2}$$

where $\boldsymbol{D}_i = (d_{i1}, d_{i2}, \ldots, d_{in_i})^T$ is a vector with the indexes for the ith individual, $m(\boldsymbol{D}_i) = E(\eta(\boldsymbol{D}_i))$ is the mean function and $K_i(\boldsymbol{D}_i, \boldsymbol{D}_i) = Cov(\eta(\boldsymbol{D}_i), \eta(\boldsymbol{D}_i)) = E(\eta(\boldsymbol{D}_i), \eta(\boldsymbol{D}_i)) - m(\boldsymbol{D}_i)m(\boldsymbol{D}_i)$ is the kernel of the process, in which $K_i(d_{ik}, d_{ij})$ is the covariance between $\eta(d_{ik})$ and $\eta(d_{ij})$, indexed by elements d_{ik} and d_{ij}, respectively. Under this definition and considering the studied case, $\eta(d_{ij})$ would be the propagation time of the ith ultrasonic wave at the d_{ij} distance, for $i = 1, \ldots, 230$ and $j = 1, \ldots, 6$.

A GP is a nonparametric model and an overview and some applications of this method are shown by Karch et al. (2020); Schulz et al. (2018); Lizotte et al. (2007); Rasmussen (2003). The mean function is usually a null function and many options are available for the kernel of the process.

Let $\boldsymbol{y} = (\boldsymbol{y}_1^T, \ldots, \boldsymbol{y}_m^T)^T$ be the observed data where $\boldsymbol{y}_i = (y_{i1}, \ldots, y_{in_i})^T$, for $i = 1, \ldots, m$, and y_{ij} is the observation of the ith individual in the jth measurement of the experiment, for $j = 1, \ldots, n_i$. As we have other variables besides the distances where the propagation time was measured, a regression model that considers a Gaussian process for incorporating correlation between observations for the same individual and fitting a nonlinear function between them (Shi and Choi, 2011) may be defined as

$$\boldsymbol{Y}_i = \boldsymbol{X}_i\boldsymbol{\beta} + \eta(\boldsymbol{D}_i) + \boldsymbol{\epsilon}_i, \tag{3}$$

where $\boldsymbol{\beta}$ is the $(p \times 1)$ vector of fixed effects; $\boldsymbol{X}_i$ is the $(n_i \times p)$ design matrix associated with fixed effects; $\eta(\cdot) \sim \text{GP}(\mathbf{0}; K_i)$; $\boldsymbol{D}_i = (d_{i1}, d_{i2}, \ldots, d_{in_i})^T$ is a vector of indexes for defining the process of the ith curve; and $\boldsymbol{\epsilon}_i$ is the $(n_i \times 1)$ vector of random errors for the ith individual. Under this new definition, $\eta(\boldsymbol{D}_i)$ represents how much the propagation time curve of the ith ultrasonic wave differs from the general average behavior given by $\boldsymbol{X}_i\boldsymbol{\beta}$, for $i = 1, \ldots, 230$.

We assume that $\boldsymbol{\epsilon}_i \sim Normal(\mathbf{0}, \sigma^2\mathbf{I})$ and random errors $(\boldsymbol{\epsilon}_i)$ and Gaussian process $(\eta(\boldsymbol{D}_i))$ are independent. Therefore, $\boldsymbol{Y}_i \sim Normal_{n_i}(\boldsymbol{X}_i\boldsymbol{\beta}, K_i + \sigma^2\mathbf{I})$, where K_i is a $(n_i \times n_i)$ variance–covariance matrix whose each element represents the covariance between each pair of observations calculated through the chosen kernel function. Thus, it follows that:

$$\begin{gathered} \boldsymbol{Y}_i|\eta(\boldsymbol{D}_i) \sim Normal_{n_i}\big(\boldsymbol{X}_i\boldsymbol{\beta} + \eta(\boldsymbol{D}_i), \sigma^2\mathbf{I}\big); \text{ and} \\ \eta(\boldsymbol{D}_i) \sim Normal_{n_i}(\mathbf{0}, K_i). \end{gathered} \tag{4}$$

Note that the marginal distribution of the defined mixed model and Gaussian process are equivalent for the observed sample if $K_i = \boldsymbol{Z}_i\boldsymbol{G}\boldsymbol{Z}_i^T$. However, as we define the elements of K_i through a specific function (kernel) which measures the covariance between a pair of observations, it is unlikely to be the same as the structure $\boldsymbol{Z}_i\boldsymbol{G}\boldsymbol{Z}_i^T$ which depends on variables. The equivalence between the models is not true for the conditional distribution, since the random effects and the elements of the Gaussian process are predicted differently.

Gibbs (1998) presents two types of kernels: the stationary type, which takes into account only the position of the observations, and the non-stationary type. A common choice in the literature is the kernel obtained by the exponentiated quadratic function, defined as

$$K_i(k, j) = \alpha_i^2 \exp\left\{-\frac{1}{2\rho_i^2}(d_{ik} - d_{ij})^2\right\}, \tag{5}$$

where $\alpha_i > 0$ and $\rho_i > 0$ are parameters to be estimated. The kernel function parameters can be the same for all individuals or for some that are correlated or homogeneous under some conditions. This kernel function is stationary and matches the purpose of this study.

Also adopting a Bayesian approach for estimating this model, prior are specified as:

- $\phi = \frac{1}{\sigma^2} \sim Gamma(\lambda_1, \lambda_2)$;
- $\boldsymbol{\beta} \sim Normal_p(\mathbf{0}, \sigma_\beta^2\mathbf{I})$;
- $\alpha_i \sim truncated - Normal(0, \sigma_\alpha^2)$; and
- $\rho_i \sim Inverse - Gamma(\lambda_{\rho 1}, \lambda_{\rho 2})$,

where $\lambda_1 > 0$, $\lambda_2 > 0$, $\sigma_\beta^2 > 0$, $\sigma_\alpha^2 > 0$, $\lambda_{\rho 1} > 0$ and $\lambda_{\rho 2} > 0$ are known hyperparameters and the *Gamma* distribution is parameterized such that $E[\phi] = \frac{\lambda_1}{\lambda_2}$. As usual in the literature, all hyperparameters are considered independent of each other.

Given the model, we are interested in the posterior inference for parameters conditioned on data. For this purpose, the likelihood function is combined with the priors to obtain the

joint posterior distribution for parameters. To estimate them, we use the Hamiltonian Monte Carlo algorithm (Neal, 2011) for simulating samples of the parameters from the joint posterior distribution and obtaining an approximation for their average and percentiles. This methodology is implemented using the Stan language through the R (R Core Team, 2024) package rstan (Stan Development Team, 2024).

3.3 Predictions

Sometimes, the interest lies in finding an estimate for models parameters, making it possible to predict the response variable for new inputs. Other times, the interest lies in identifying factors that influence the behavior of the response variable, as is the goal of this work. However, a model capable of effectively predicting new inputs usually is a good model to study the impact of factors on the response variable as well. Thus, out-of-sample prediction has also been successfully used to assess the quality and suitability of models and compare them.

Following Sela and Simonoff (2012), we may be interested in three types of prediction: 1—predicting new observations for individuals in the sample; 2—predicting observations for new individuals for whom there are no early observations of the response; and 3—predicting new observations for new individuals for which early observations are available but which were not considered in the model estimation.

Let $\star$ represents new observations for j and/or i. In a mixed model and for the first sort of prediction, we predict $\boldsymbol{y}_{i\star}$ as $\boldsymbol{X}_{i\star}\hat{\boldsymbol{\beta}} + \boldsymbol{Z}_{i\star}\hat{\boldsymbol{b}}_i$, for $i = 1, 2, \ldots, m$, since both fixed and random effects estimates and predictions are available from the estimation process. For the second sort of prediction, we have no basis for predicting $\boldsymbol{b}_\star$ and we predict $\boldsymbol{y}_{\star\star}$ as its marginal expected value given by $\boldsymbol{X}_{\star\star}\hat{\boldsymbol{\beta}}$. In the third case, we may use available observations of the response variable to estimate $\boldsymbol{b}_\star$ based on the fitted model and carry out the prediction as in the first sort of prediction for new observations. The random effects for a new individual for whom there are some early observations of the response and it was not considered in the model fitting may be estimated by applying Eq. (3.2) of Laird and Ware (1982) or as the average from its full conditional posterior distribution.

Considering a GP, we can write the joint distribution of the n_i observed values and the $n_{i\star}$ function values at the prediction locations for a specific individual as

$$\begin{bmatrix} \boldsymbol{Y}_i \\ \eta(\boldsymbol{d}_{i\star}) \end{bmatrix} \sim Normal\left(\begin{bmatrix} \boldsymbol{X}_i\boldsymbol{\beta} \\ \boldsymbol{0} \end{bmatrix}, \begin{bmatrix} K_i(\boldsymbol{D}_i, \boldsymbol{D}_i) + \sigma^2\mathbf{I} & K_i(\boldsymbol{D}_i, \boldsymbol{d}_{i\star}) \\ K_i(\boldsymbol{d}_{i\star}, \boldsymbol{D}_i) & K_i(\boldsymbol{d}_{i\star}, \boldsymbol{d}_{i\star}) \end{bmatrix}\right),$$

where $K_i(\boldsymbol{D}_i, \boldsymbol{d}_{i\star})$ denotes the $(n_i \times n_{i\star})$ matrix of covariances evaluated at all pairs of estimation and prediction points of the ith individual, and similarly for the other entries of $K_i(\cdot, \cdot)$. Using the properties of the multivariate $Normal$ distribution, the predictive distribution for $\eta(\boldsymbol{d}_{i\star})$ is given by

$$\eta(\boldsymbol{d}_{i\star}) \mid \boldsymbol{D}_i, \boldsymbol{y}_i, \boldsymbol{d}_{i\star} \sim Normal_{n_{i\star}}(\boldsymbol{\mu}_{\eta|\boldsymbol{y}_i}, \boldsymbol{\Sigma}_{\eta|\boldsymbol{y}_i}),$$

where $\boldsymbol{\mu}_{\eta|\boldsymbol{y}_i} = K_i(\boldsymbol{d}_{i\star}, \boldsymbol{D}_i)[K_i(\boldsymbol{D}_i, \boldsymbol{D}_i) + \sigma^2\mathbf{I}]^{-1}(\boldsymbol{y}_i - \boldsymbol{X}_i\boldsymbol{\beta})$ and $\boldsymbol{\Sigma}_{\eta|\boldsymbol{y}_i} = K_i(\boldsymbol{d}_{i\star}, \boldsymbol{d}_{i\star}) - K_i(\boldsymbol{d}_{i\star}, \boldsymbol{D}_i) \times [K_i(\boldsymbol{D}_i, \boldsymbol{D}_i) + \sigma^2\mathbf{I}]^{-1}K_i(\boldsymbol{D}_i, \boldsymbol{d}_{i\star})$ as described by Williams and Rasmussen (2006). Therefore, new observations for the ith individual, $\boldsymbol{y}_{i\star}$, are predicted as $\boldsymbol{X}_{i\star}\hat{\boldsymbol{\beta}} + \hat{\boldsymbol{\mu}}_{\eta|\boldsymbol{y}_i}$, for $i = 1, 2, \ldots, m$. The third sort of prediction in GP may be done straightforward as this first but based on the early observations of this new individual and assuming the estimated kernel function of a similar curve.

Observations for new individuals for whom there are no early observations of the response may also be predicted similarly to before, but considering the entire estimation data. That is,

using $\boldsymbol{y}$ instead of $\boldsymbol{y}_i$ and $\boldsymbol{D}$ instead of $\boldsymbol{D}_i$, or some subset of them that is more homogeneous to the individuals to be predicted.

4 Results

We estimate the mixed model and the Gaussian process using the five first measures and leave the last measure (at the distance of 35 cm) of each wave out to analyze the predictive capacity of the fitted models and compare their quality and suitability. For both models, we consider as factors 7 variables (features) with fixed effects, as follows:

- X_1: height of each measurement;
- X_2: binary variable that indicates if the measurement is made on the brick–grout interface or not;
- X_3: binary variable that indicates if the measurement is made on the brick with void in its way or not;
- X_4: binary variable that indicates if the measurement is made on the brick with no voids in its way or not;
- X_5: distance of each measurement from the origin of the wave;
- X_6: squared distance of each measurement from the origin of the wave; and
- X_7: cubic distance of each measurement from the origin of the wave.

In the mixed model, we also consider the regression coefficients of distance variables and intercept as random effects for each wave. It allows different waves to have different cubic functions between the distances traveled while the mean curve of the propagation time is modeled by the fixed effects. This definition of the variables associated with random effects also allows, due to the marginal variance structure of $\boldsymbol{Y}_i$, the propagation time at different distances to present different variances. In this case, as the linear, quadratic and cubic distance are considered in $\boldsymbol{Z}_i$, the greater the distance of a specific measurement, the greater the variability of its propagation time, which is the behavior observed in the analyzed data. We discuss this more later.

Observe that, we write the propagation time of waves as a cubic polynomial function of the distance. We choose a polynomial of degree 3 because it is flexible enough and relatively simple for modeling the observed curves of the experimental data set. In order to avoid multicollinearity among distance variables, we use the orthogonal version of them instead of x_{5ij}, x_{5ij}^2 and x_{5ij}^3, and leave the element grout as the reference category to be compared with brick–grout interface, brick with no voids in the wave way and brick with voids in the wave way categories. Our main goal is to identify if and which of these factors are relevant and influence the behavior of ultrasonic waves on masonry walls.

For the Gaussian process, we consider the distance of each measurement from the origin as the index variable to model the correlation among the observations for each wave. We also assume only one kernel function for each frame in a total of 24 different kernel functions. That is, different waves from the same frame share the same kernel function and its parameters. It makes sense since waves from the same frame are propagated and measured in the same path and should show similar correlation behavior among their measurements. We estimate a GP allowing distinct kernel functions for each wave as well, but the results for variable selection and out-of-prediction are not good and we do not show them here.

We fix the hyperparameters $\lambda_1 = \lambda_2 = 0.01$, $v = 5$, $\boldsymbol{W} = \text{diag}(100)$, $\sigma_\beta^2 = 1{,}000{,}000$, $\sigma_\alpha^2 = 100$, $\lambda_{\rho 1} = 3$ and $\lambda_{\rho 2} = 5$ in order to have vague prior distributions with large variance. We run the algorithms 20,000 iterations, discarding the first 5,000 iterations as burn-in period

Table 1: Regression coefficients estimates (point and interval estimates—90% credibility interval). In bold, we highlight the most relevant difference between the fitted models.

Parameter (factor)	MM	GP
β_0 (Intercept)	127.47(117.51, 136.42)	109.95(105.13, 114.62)
β_1 (X_1)	9.54(4.52, 14.22)	5.56(0.78, 10.67)
β_2 (X_2)	5.26(1.25, 8.86)	9.05(4.84, 13.47)
β_3 (X_3)	**9.76(5.73, 13.88)**	**−3.58(−7.15, −0.17)**
β_4 (X_4)	7.52(3.90, 11.23)	12.29(7.74, 16.69)
β_5 (X_5)	195.56(171.74, 217.23)	136.24(130.95, 141.62)
β_6 (X_6)	31.97(17.09, 46.45)	5.97(1.79, 10.69)
β_7 (X_7)	5.98(−0.82, 12.66)	1.22(−1.81, 4.34)
σ^2	171.67(153.15, 193.02)	48.43(37.7, 64.00)

and thinning out to save every 10th iteration. We verify the convergence and mixing of chains through trace plots and Geweke's convergence metric available in R package of Plummer et al. (2006).

Table 1 displays the estimates for each fixed regression coefficient and the random error variance of the fitted models. From both models, we observe that the average relationship between the distance traveled and the propagation time of the ultrasonic wave in masonry walls is not linear, as expected when waves propagate through heterogeneous material. This is because the fixed effect for the squared distance (X_6) is relevant, and its credibility interval does not contain the zero value. However, the effect for the cubic distance (X_7), despite presenting a positive point estimate, includes the zero value in its credibility interval. Therefore, the cubic distance is not relevant for describing the average behavior of the waves up to the fifth measured point and will be omitted from the modeling.

The height of the measurements has a positive effect in both models. It indicates that the higher the measurement, the slower the propagation of the wave, since the propagation time increases on average. As expected, the material through which the wave propagates influences the behavior of its propagation time. This can be observed by examining the estimated coefficients of X_2, X_3, and X_4, which are all relevant (compared with the grout category left out as the reference) for both models at the 90% credibility level. If we consider the 95% credibility level, which is also very traditional, the difference in the interval limits is generally in the first decimal place. For β_3 in GP, the 95% credibility interval is $(-7.70, 0.28)$ which contains the zero value, but it is predominantly allocated to negative values.

According to the mixed model and considering binary variables, the tendency is that waves on the brick with voids are the slowest (X_3), followed by waves on the brick without voids (X_4) and on the brick–grout interface (X_2). This is because the wave travels faster on the grout, which was left out as a reference and, consequently, on the interface that contains grout in its composition.

For GP estimates, the average trend is that waves on the brick without voids (X_4) are the slowest, followed by waves on the brick–grout interface (X_2), waves on the grout, and waves propagated on the brick with voids (X_3), which seem to be the fastest or very similar (if we consider the 95% credibility interval) to the spread on the grout of the masonry wall. We also change the exponentiated quadratic kernel that provides smooth realizations to the exponential kernel (with power equal to 1) that gives much rougher realizations to analyze their impact on

parameters estimation for the GP. Both functions are extreme cases of the power exponentiated kernel. We do not show here all the results for the exponential kernel as we do for the exponentiated quadratic kernel, but the estimates (point and credibility interval) for the regression coefficients are very similar. In general, the differences are in the first or second decimal place. The biggest difference is in the estimation of the σ^2 whose estimate using the new kernel is 10.86 (5.02,25.91). The convergence of the algorithm using the exponential kernel was slower and more difficult to achieve.

The greatest divergence between the two fitted models is the estimate of the fixed effect for measurements made on bricks with voids. The mixed model presents a positive regression coefficient, while GP estimates a negative regression coefficient for the factor X_3. This is probably due to the fact that the mixed model, unlike the Gaussian process, better captured the initial behavior of the waves in its fixed effects (when most waves had not yet reached the part of the brick with voids).

Other parameters involved in the mixed model are the variances and covariances of the random effects represented in the $\boldsymbol{G}$ matrix. As we consider four random effects: the intercept and the regression coefficients for the orthogonal version of the linear, squared and cubic distance, this matrix has 4×4 dimension. Its point estimate is given by

$$\widehat{\boldsymbol{G}} = \begin{bmatrix} 3572.93 & 9625.53 & 5393.10 & 1923.76 \\ 9625.53 & 27057.94 & 16172.38 & 6099.98 \\ 5393.10 & 16172.38 & 10649.09 & 4318.96 \\ 1923.76 & 6099.98 & 4318.96 & 1854.68 \end{bmatrix}.$$

We note that the random effect associated to the linear distance (second column) is the one with the greatest variance and the one associated with the cubic distance (fourth column) has the lowest variance. See also the first panel in Figure 4. The marginal variance of each $\boldsymbol{Y}_i$ is then estimated as

$$\widehat{Var}(\boldsymbol{Y}_i) = \begin{bmatrix} 197.15 & 22.06 & 59.29 & 93.59 & 82.06 & -18.46 \\ 22.06 & 273.85 & 145.76 & 327.89 & 817.38 & 1788.99 \\ 59.29 & 145.76 & 591.21 & 776.43 & 1112.73 & 1325.56 \\ 93.59 & 327.89 & 776.43 & 1778.40 & 2972.74 & 5045.93 \\ 82.06 & 817.38 & 1112.73 & 2972.74 & 8530.90 & 19290.67 \\ -18.46 & 1788.99 & 1325.56 & 5045.93 & 19290.67 & 50731.68 \end{bmatrix}$$

and its corresponding standardized matrix that shows the correlation between measurements at different distances is given by

$$\begin{bmatrix} 1.00 & 0.10 & 0.17 & 0.16 & 0.06 & -0.01 \\ 0.10 & 1.00 & 0.36 & 0.47 & 0.54 & 0.48 \\ 0.17 & 0.36 & 1.00 & 0.76 & 0.49 & 0.24 \\ 0.16 & 0.47 & 0.76 & 1.00 & 0.76 & 0.53 \\ 0.06 & 0.54 & 0.49 & 0.76 & 1.00 & 0.93 \\ -0.01 & 0.48 & 0.24 & 0.53 & 0.93 & 1.00 \end{bmatrix}.$$

Through the $\widehat{Var}(\boldsymbol{Y}_i)$, we observe the flexibility of the assumed mixed model in modeling and describing the heteroscedasticity present in the analyzed data. We note on the main diagonal that the marginal variance of the measurements increases as the distance from the origin increases. As observed at Figure 5, the measurements at distance 35 cm vary much more than measurements

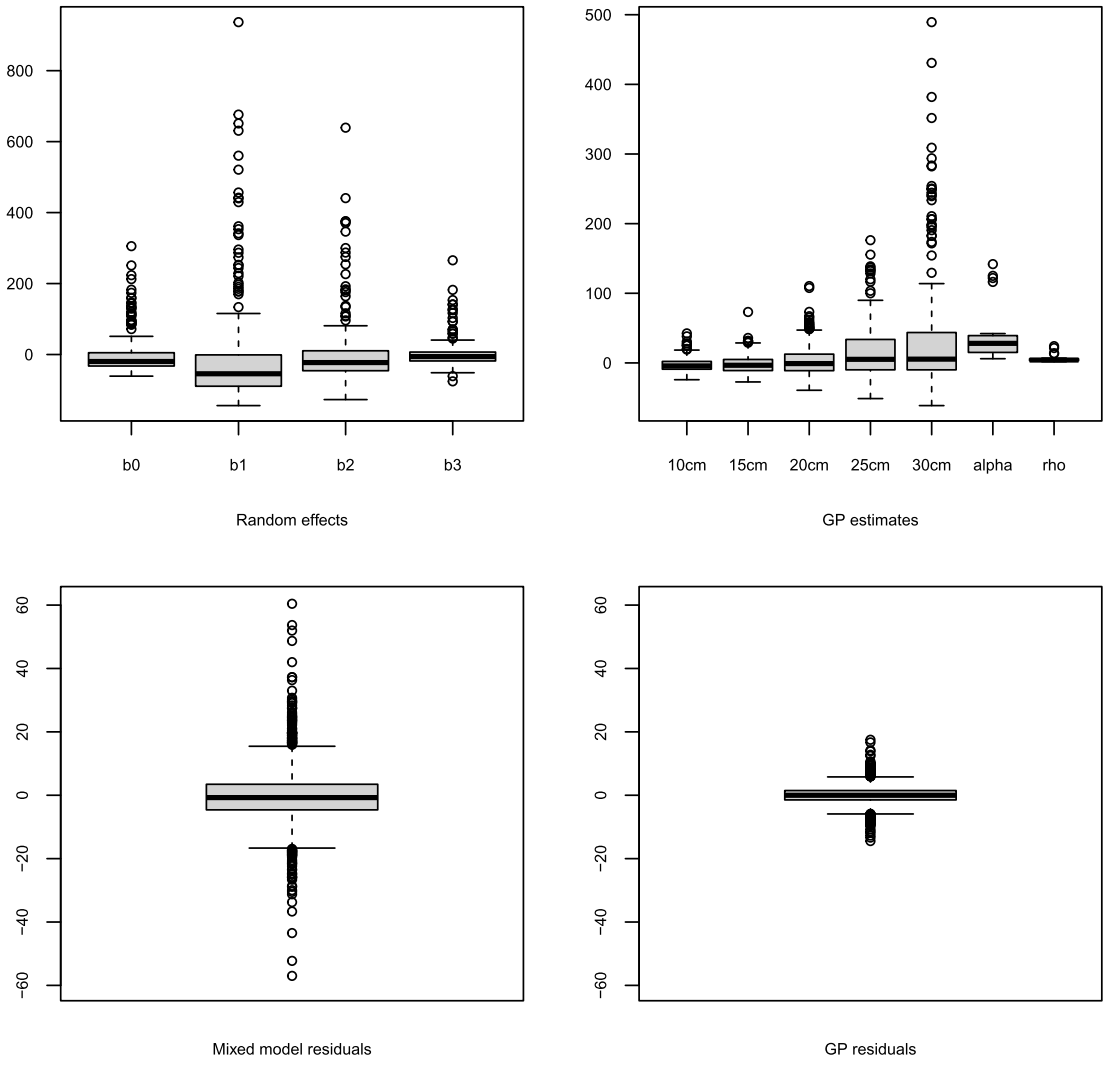

Figure 4: Predictions and conditional residuals for MM (first column) and GP (second column).

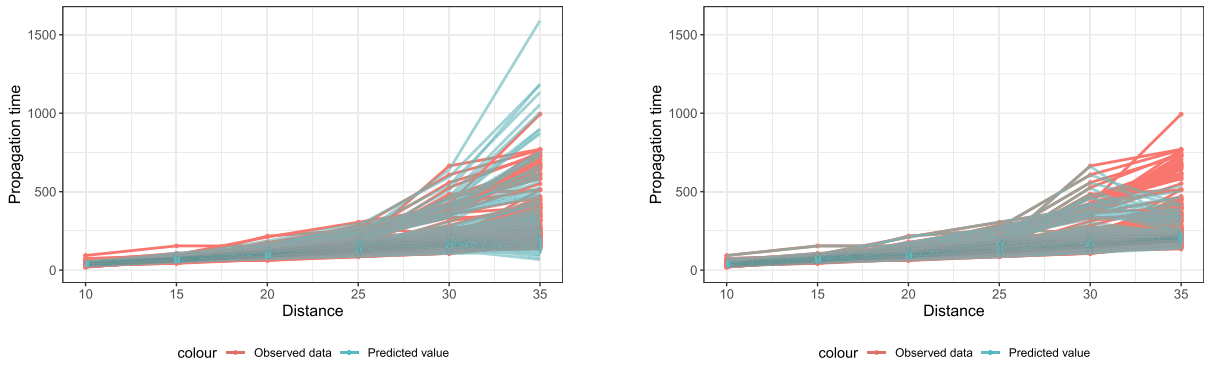

Figure 5: Observed curves (red) and predicted curves (green). On left size we show the MM prediction and, on the right size, the GP prediction.

at distance 10 cm. From the correlation matrix, we observe that close measurements are, in general, more correlated and more distant measurements are less correlated, as it was expected.

The Gaussian process for each of the 24 frames, in turn, involves two parameters: the parameter α, where α^2 is known as the overall variance for the process, and the lengthscale ρ. Their point estimates are shown in the top right panel of Figure 4. The lowest estimated value of α is $6.06(1.75, 9.60)$ (in parentheses the 95% credibility interval) and the greatest is $141.95(115.20, 179.13)$. The lowest estimated value of ρ is $1.79(0.68, 3.20)$ and the greatest is $23.91(13.50, 39.80)$. Considering the model with $\widehat{\rho} = 1.79$ and its associated $\widehat{\alpha} = 33.71$, the correlation between measurements with a distance of 1, 2, 3, 4, 5 and 10 cm is, respectively, 0.86, 0.54, 0.25, 0.08, 0.02 and < 0.0001. For the case where $\widehat{\rho} = 23.91$ and its associated $\widehat{\alpha} = 39.61$, the correlation between measurements with a distance of 1, 5, 10 and 20 cm is, respectively, 0.999, 0.978, 0.916, and 0.705. Low correlations (< 0.05) are only observed in the latter case between measurements with a distance greater than 59 cm.

Before analyzing the predictive capacity of fitted models, we carry out a simple diagnostic analysis to briefly check some models assumptions and verify their suitability in describing the behavior of the data. We focus on analyzing the conditional residuals to verify random error properties and the predicted random effects and Gaussian process elements to check assumptions for them.

The first column of Figure 4 shows the prediction of random effects and conditional residuals for the MM. Although there are outliers, the distributions of them, shown through boxplots, are apparently symmetrical around zero value as it is expected for following a *Normal* distribution with zero mean. Predictions of random effects b_{i1}, that are associated with the linear distance, are the most variable and far from the zero value while the predictions for b_{i3}, which are associated with the cubic distance, are the closest to zero value. It represents that few curves need the cubic order to describe their behavior through the MM.

The second column of Figure 4 shows the prediction of elements and conditional residuals for the GP, in addition to point estimate of its kernel parameters. Again, although there are outliers, the distributions of conditional residuals and elements of GP for each distance are apparently symmetrical around zero value as it is expected for following a *Normal* distribution with zero mean. The predictions of the GP elements for greater distances are those further from the zero value and with more outliers since they are the distances that present behavior more different from the average behavior.

We do not show them here, but we also analyze the graphs of conditional residuals versus observation index for MM and GP. We observe that, despite the outliers, the residuals exhibit homoscedastic behavior, as assumed for random errors in the models. Therefore, although the conditional residuals of GP are smaller than those of MM (see Figure 4), we consider that both fits are satisfactorily suitable to describe the general behavior of the data.

To choose the fitted model most suitable for the data, mainly because they do not agree about the average behavior of waves propagated on bricks with voids, we evaluate their predictive performance in all distances traveled. The models are also evaluated at the distance 35 cm that was not used in their estimation. Figure 5 shows the observed and predicted propagation time for both models. We observe that, when considering the distances used to fit the models, both methods predict the propagation time well and the GP is a little more accurate.

In the out-of-sample distance, we note a prevalence of lower predictions than observed values for both models, although the mixed model predicts some greater values for slower curves with very atypical behavior. Despite the mixed model predicting better atypical behaviors, the GP seems to predict better the average and general behaviors. Especially, the GP better captured

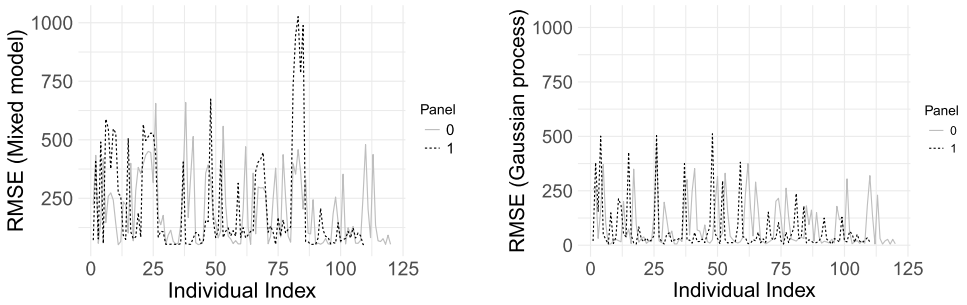

Figure 6: Root mean square error (RMSE) for predicting the propagation time at the distance of 35 cm for each curve. On the left side, we show the results of the mixed model and, on the right side, the results of the Gaussian process.

the behavior for faster and more linear curves, which is the case of waves propagated on voids or grout. The measurement made on the brick with voids in its way has a small difference in relation to the measurement done on the grout, left out as the reference, for GP. This means that, in this case, the average behavior of the wave is more similar to the average behavior of the measurements on the grout. It confirms that, in the presence of voids, the wave seems to travel through the coating grout. Predictions for the mixed model are more variable than GP predictions, and this also reflects on the mean squared error of predictions shown in Figure 6.

Figure 6 presents the root mean square error (RMSE) for predicting measurements left out of the models fitting. For each wave, we calculate the RMSE based on its forecast on each MCMC iteration. This figure shows the RMSE for waves in the wall without voids (Panel 0) and for waves in the wall with voids (Panel 1). The figure shows that, in general, mixed model RMSEs are greater than GP RMSEs. RMSE values for the wall with anomalies also seem to be greater than the values for the preserved wall when considering the mixed model.

The GP fitted here, although it does not predict very well atypical behaviors, describes the average final behavior of the waves better through its fixed effects (when all the curves have already reached the part of the brick with voids), as shown in Figure 5. We observe that the GP similarly predicts the last measurements on the wall with and without voids (see the right graphic of Figure 6), probably because this model better captured the difference between their average curves.

As we discussed in the data presentation, one curve from the fourth frame of P2 with only 4 measurements instead of 6 was also omitted in the models estimation. In it we check the performance of the second and third type of prediction for both models. Figure 7 shows the predictions and 95% prediction intervals. For distances that have observed measurements, we note that GP predictions are more precise and the prediction intervals, despite being much smaller than MM intervals, contain the observed values. The severe growth in the type-II prediction of distances 30 and 35 cm for the GP follows the behavior observed in other curves in this same frame used for prediction. Note that for type-III prediction, when we only consider the four available measurements of this curve for predicting future missing observations, this does not happen and a smooth curve is predicted.

Considering all comments and previous analyses, and that the GP model is more in agreement with descriptive analysis, we conclude that, under the considered dataset, this model is more suitable for identifying the relevant factors and their effects on ultrasonic wave propagation inside masonry walls.

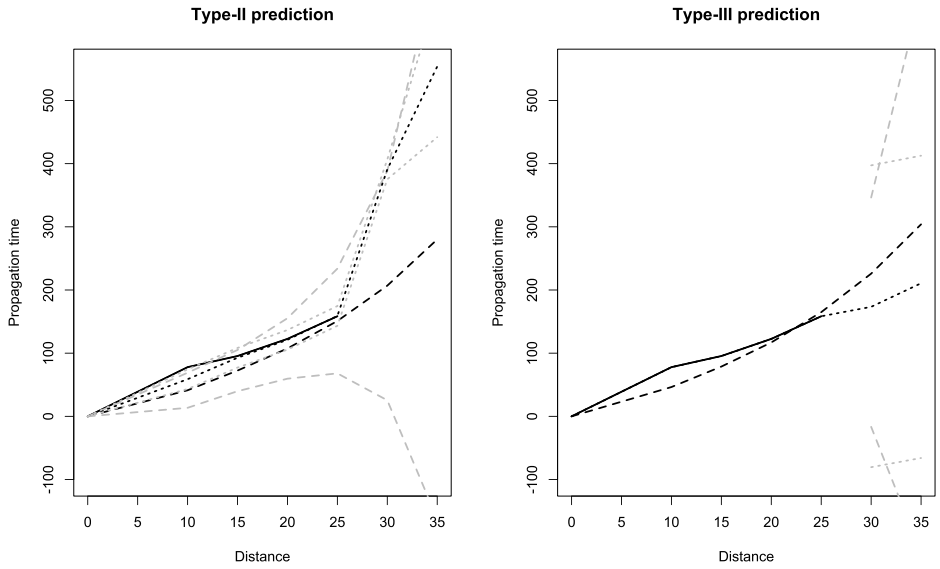

Figure 7: Observed and predicted measurements for the incomplete curve. Solid line represents observed values, dashed lines represent MM predictions and dotted lines represent GP predictions. The gray lines are the prediction intervals.

In addition to identifying that the material and its quality over which the wave propagates alter the behavior and propagation time of the wave, we conclude that waves propagated in a way with voids are, on average, the fastest and present behavior closer to the waves propagated over the grout. As this goes against physical laws, it is likely that when the wave encounters a void, instead of continuing to propagate through the brick, it propagates through the grout that is on the wall cover. Although this is an assumption and more experiments are needed to confirm it, we demonstrate that the material and its quality on which the ultrasonic wave is propagated changes its behavior, and the wave propagation behavior may be useful to predict the quality of the material in its way.

5 Discussion

We employed a mixed model and Gaussian process to describe the propagation behavior of ultrasonic waves inside masonry walls, which are traditional statistical models for analyzing correlated data. Our main objective through these methods is to adequately describe the relationship between the distance traveled and the propagation time of the waves and to identify factors that impact this behavior. If it is identified that the wave behavior changes according to certain features of the wall, as we have observed, the propagation behavior of waves may be used in future studies to classify the quality of a wall without resorting to destructive methods. In this sense, classification models, such as random forests, neural networks, multinomial logistic regressions, among others, could be fitted using propagation time at different distances and other features as covariates to predict wall quality in distinct parts. Further experiments under more detailed and specific conditions would be needed to collect data for this modeling.

Both the mixed model and the gaussian process capture that the relationship between the distance traveled by an ultrasonic wave and its propagation time is not linear in masonry walls,

as expected when a wave is propagated in a heterogeneous material. The height and the material condition where the wave is propagated change, on average, its behavior. Ultrasonic waves that are propagated on preserved bricks are usually slower and present the most heterogeneous and atypical behavior. Ultrasonic waves that are propagated on the grout are usually faster and present the most homogeneous and linear behavior.

Thus, for the GP model, the fixed coefficient referring to the brick with void has less relevance when compared with propagation on the grout. This suggests that the wave may propagate through the wall coating if there is a void inside. However, this is an assumption, and more experiments are needed to confirm whether or not this is a general behavior for this type of wave and material.

Based on the predictive performance and diagnostic analysis, we conclude that, under the analyzed data, the GP model better describes the average and general behavior of the waves, while the mixed model better captured atypical behaviors. It is possible that the GP would provide good results in a classification model, outperforming the mixed model most commonly used in the literature. This type of information is crucial for developing any automated system dedicated to monitoring masonry construction. The effectiveness of such a system is heavily dependent on the precision and quality of the employed model, which, in turn, relies on the inclusion of relevant external information.

Supplementary Material

The data that support this study are openly available in a public repository on Github at https://github.com/larebufc/ultrasonic-data-analysis as well as the R and Stan codes used for implementing the methodologies.

References

ABNT (2020). *NBR 16805*. Associação Brasileira de Normas Técnicas, Rio de Janeiro - Brazil.

Araújo E, Sousa I, Paz R, Costa CH, Mesquita E (2020). Physical and mechanical characterization of traditional Brazilian clay bricks from different centuries. *Journal of Building Pathology and Rehabilitation*, 5(1): 1–12. https://doi.org/10.1007/s41024-019-0067-3

Banerjee S, Gelfand AE, Finley AO, Sang H (2008). Gaussian predictive process models for large spatial data sets. *Journal of the Royal Statistical Society, Series B, Statistical Methodology*, 70(4): 825–848. https://doi.org/10.1111/j.1467-9868.2008.00663.x

Binda L, Saisi A, Zanzi L (2003). Sonic tomography and flat-jack tests as complementary investigation procedures for the stone pillars of the temple of s. Nicolò l'Arena (Italy). *NDT & E International*, 36(4): 215–227. Structural Faults and Repair. https://doi.org/10.1016/S0963-8695(02)00066-X

Cheng L, Ramchandran S, Vatanen T, Lietzén N, Lahesmaa R, Vehtari A, et al. (2019). An additive gaussian process regression model for interpretable non-parametric analysis of longitudinal data. *Nature Communications*, 10(1): 1–11. https://doi.org/10.1038/s41467-018-07882-8

Ebden M (2015). Gaussian processes: A quick introduction. arXiv preprint: https://arxiv.org/abs/1505.02965.

Edwards LJ, Stewart PW, MacDougall JE, Helms RW (2006). A method for fitting regression splines with varying polynomial order in the linear mixed model. *Statistics in Medicine*, 25(3): 513–527. https://doi.org/10.1002/sim.2232

Gibbs MN (1998). Bayesian gaussian processes for regression and classification. Ph.D. thesis, University of Cambridge.

Grimm K, Zhang Z, Hamagami F, Mazzocco M (2013). Modeling nonlinear change via latent change and latent acceleration frameworks: Examining velocity and acceleration of growth trajectories. *Multivariate Behavioral Research*, 48(1): 117–143. https://doi.org/10.1080/00273171.2012.755111

Grimm KJ, McArdle JJ, Hamagami F (2007). Nonlinear growth mixture models in research on cognitive aging. In: *Longitudinal Models in the Behavioral and Related Sciences* (K AS, van Montfort, J Oud, eds.). Lawrence Erlbaum Associates Publishers.

Grimm KJ, Ram N, Estabrook R (2016). *Growth Modeling: Structural Equation and Multilevel Modeling Approaches*. Guilford Publications.

Karch JD, Brandmaier AM, Voelkle MC (2020). Gaussian process panel modeling—machine learning inspired analysis of longitudinal panel data. *Frontiers in Psychology*, 11: 351. https://doi.org/10.3389/fpsyg.2020.00351

Kot P, Muradov M, Gkantou M, Kamaris GS, Hashim K, Yeboah D (2021). Recent advancements in non-destructive testing techniques for structural health monitoring. *Applied Sciences*, 11(6): 2750. https://doi.org/10.3390/app11062750

Laird NM, Ware JH (1982). Random-effects models for longitudinal data. *Biometrics*, 38(4): 963–974. https://doi.org/10.2307/2529876

Lizotte DJ, Wang T, Bowling MH, Schuurmans D (2007). Automatic gait optimization with Gaussian process regression. In: *IJCAI*, volume 7, 944–949.

Mesquita E, Martini R, Alves A, Mota L, Rubens T, Antunes P, et al. (2018). Heterogeneity detection of Portuguese–Brazilian masonries through ultrasonic velocities measurements. *Journal of Civil Structural Health Monitoring*, 8(5): 847–856. https://doi.org/10.1007/s13349-018-0312-5

Miranda L, Cantini L, João Guedes J, Binda L, Costa A (2013). Applications of sonic tests to masonry elements: Influence of joints on the propagation velocity of elastic waves. *Journal of Materials in Civil Engineering*, 25(6): 667–682. https://doi.org/10.1061/(ASCE)MT.1943-5533.0000547

Neal RM (2011). MCMC using Hamiltonian dynamics. *Handbook of Markov Chain Monte Carlo*, 2: 113–162. https://doi.org/10.1201/b10905-6

Plummer M, Best N, Cowles K, Vines K (2006). CODA: Convergence diagnosis and output analysis for MCMC. *R News*, 6(1): 7–11.

Quintana FA, Johnson WO, Waetjen LE, Gold EB (2016). Bayesian nonparametric longitudinal data analysis. *Journal of the American Statistical Association*, 111(515): 1168–1181. https://doi.org/10.1080/01621459.2015.1076725

R Core Team (2024). *R: A Language and Environment for Statistical Computing*. R Foundation for Statistical Computing, Vienna, Austria.

Rasmussen CE (2003). Gaussian processes in machine learning. In: *Summer School on Machine Learning*, 63–71. Springer.

Rodrigues AM (2009). Linear mixed models: A practical guide using statistical software. *Silva Lusitana*, 17: 123–125.

Rodrigues RV (2021a). Análise estatística de dados ultrassônicos para a seleção de características da alvenaria que comprometem sua estabilidade. Bachelor's thesis, Universidade Federal de São Carlos, Brazil.

Rodrigues TC (2021b). Análise exploratória de dados ultrassônicos para reconhecimento de

vazios em alvenarias maciças. Bachelor's thesis, Universidade Federal do Ceará, Brazil.

Schulz E, Speekenbrink M, Krause A (2018). A tutorial on Gaussian process regression: Modelling, exploring, and exploiting functions. *Journal of Mathematical Psychology*, 85: 1–16. https://doi.org/10.1016/j.jmp.2018.03.001

Sela RJ, Simonoff JS (2012). RE-EM trees: A data mining approach for longitudinal and clustered data. *Machine Learning*, 86(2): 169–207. https://doi.org/10.1007/s10994-011-5258-3

Shi JQ, Choi T (2011). *Gaussian Process Regression Analysis for Functional Data*. Chapman and Hall/CRC.

Singer JM, Andrade Dd (1986). Análise de Dados Longitudinais. *Simpósio Nacional de Probabilidade e Estatística*, 7.

Stan Development Team (2024). RStan: The R interface to Stan. R package version 2.32.6.

Valluzzi MR, Cescatti E, Cardani G, Cantini L, Zanzi L, Colla C, et al. (2018). Calibration of sonic pulse velocity tests for detection of variable conditions in masonry walls. *Construction & Building Materials*, 192: 272–286. https://doi.org/10.1016/j.conbuildmat.2018.10.073

Verstrynge E, Lacidogna G, Accornero F, Tomor A (2021). A review on acoustic emission monitoring for damage detection in masonry structures. *Construction & Building Materials*, 268: 121089. https://doi.org/10.1016/j.conbuildmat.2020.121089

Williams CK, Rasmussen CE (2006). *Gaussian Processes for Machine Learning*. MIT Press, Cambridge, MA.

Zuanetti DA, da Paz RF, Rodrigues T, Mesquita E (2021). Clustering ultrasonic waves propagation time: A hierarchical polynomial semiparametric approach. *Applied Stochastic Models in Business and Industry*, 37(5): 894–907. https://doi.org/10.1002/asmb.2609